A first application of thermographic phosphors in a marine two-stroke diesel engine for surface temperature measurement

Abou Nada, Fahd Jouda; Hult, Johan; Knappe, Christoph; Richter, Mattias; Mayer, Stefan; Aldén, Marcus

Published in:
Proceedings of the ASME 2014 Internal Combustion Engine Division Fall Technical Conference (ICEF2014)

2014

Proceedings of the 2014 Fall Conference of the ASME Internal Combustion Engine Division
ICEF2014
October 19-22, 2014, Columbus, Indiana, USA
ICEF2014-5417

A FIRST APPLICATION OF THERMOGRAPHIC PHOSPHORS IN A MARINE TWO-STROKE DIESEL ENGINE FOR SURFACE TEMPERATURE MEASUREMENT

Fahd Abou Nada[1], Johan Hult[2], Christoph Knappe[1], Mattias Richter[1], Stefan Mayer[2] and Marcus Aldén[1]
[1]Department of Physics, Division of Combustion Physics, Lund University, Box 118, S-22100, Lund, Sweden
[2] MAN Diesel & Turbo, Teglholmsgade 41, 2450 Copenhagen, Denmark

E-mail: fahed.abou_nada@forbrf.lth.se

ABSTRACT

Phosphor thermometry is applied for the first time in a large-bore two-stroke diesel engine. The work proves the practicality of phosphor thermometry in large-bore engines. The experiments were conducted on the MAN 4T50ME-X marine research engine equipped with an optical cylinder head. By employing a thin surface coating of $CdWO_4$ phosphor, cycle resolved temperature measurements of the cylinder wall were obtained. Motored and fired engine operations were tested at engine loads covering the low and medium engine load range. Phosphor thermometry proved to be successful in retrieving the temperature with standard deviations ranging around 1-8 K. Experimental considerations like detector linearity, coating thickness and an automated phosphor calibration routine will be addressed.

Keywords: Thermographic phosphors, Laser-induced phosphorescence, Marine propulsion, Large-bore two-stroke diesel engines

INTRODUCTION

Around 90 percent of the global trade is carried overseas using a huge fleet of ships [1]. The introduction of tier I emission standards in 2000 signified the beginning of an era of strict NO_x, SO_x and particulate matter ship emission limits. Later on, tier II came into effect in 2011 enforcing even more stringent emission limits. Even lower limits, tier III emission standards, are expected to take effect in 2016.

Since the vast majority of the marine vessels depend on heavy fuel oil, as the sole means of propulsion, there is an ever increasing demand for more environmentally sound marine engines. This demand is compelled by the implementation of more stringent legislations lowering the emission limits. In addition, the increase in oil prices necessitates more efficient engines to keep the economic cost of running the ship fleet at a competitive level.

Increasing the efficiency and the specific power of internal combustion (IC) engines can be achieved by increasing their compression ratio and boost level. Latest generation large-bore two-stroke diesel engines typically operate at higher pressures, particularly at part load, than previous generations. This can lead to changes in cylinder heat-loads, and monitoring of surface temperatures on critical components is thus of large importance. Knowledge of combustion chamber component temperatures is also vital for developing the capability of this type of engine to run on alternative fuel sources, such as liquefied natural gas (LNG) or liquefied petroleum gas (LPG) [2].

In-cylinder temperature measurements have proven to suffer from a high level of complexity due to the fast thermal changes occurring during engine operation. Two measurement techniques are currently used to obtain temporally and spatially resolved cylinder wall temperature. The first utilizes highly responsive thermocouples, which are placed in contact with the surface whose temperature is to be measured [3-6]. Thermocouples inherently provide a highly temporally resolved zero-dimensional temperature, but positioned in a distributed cluster they can provide quasi-two dimensional data. Handling a group of thermocouples can be challenging and impractical, especially when placed on moving engine parts. The intrusiveness of thermocouples cannot be ignored when precise and accurate temperature measurements are needed.

Recently, a semi-nonintrusive temperature measurement technique known as phosphor thermometry has been employed to obtain in-cylinder temperature information. The phosphor thermometry technique exploits the temperature dependence of the phosphorescence properties to attain the temperature of the phosphor material. The observed temperature-dependent phosphor properties are the spectral intensity and the phosphorescence decay-time. The measurement methodologies employed to obtain temperature information from different thermographic phosphors have been discussed and reported extensively, see e.g. [7-10]. Several zero-dimensional and two-

dimensional, temporally resolved temperature measurements inside internal combustion engines were reported in [11-18].

This work presents temperature measurements performed on the 4T50ME-X marine research engine (MAN Diesel & Turbo, Copenhagen, Denmark) using phosphor thermometry. To the authors best knowledge this constitutes the first application of this technique in a large-bore engine. Information on in-cylinder surface temperatures from such marine engines is sparse and yet either measured by thermocouples and/or derived from sub-surface locations. This work is part of a larger experimental effort aimed at increasing understanding of in-cylinder conditions in large-bore marine diesel engines [19, 20].

EXPERIMENTAL CONSIDERATIONS

Phosphor thermometry

Thermographic phosphors (TP) react to the change of temperature by altering its phosphorescence emission characteristics. The current work is only focused on the temporal changes occurring to the phosphorescence. After exciting the thermographic phosphor with a temporally short UV-light pulse, an exponentially decaying phosphorescence signal is emitted (Eq. 1). I(t) and I_0 are the intensity of the emitted signal at any given time t and at t = 0, respectively. τ is associated with the decay-time and C is a constant signal offset. The main aspect of TPs is their high sensitivity to temperature, remoteness, and durability, allowing for temperature measurement even in harsh environments. The decay time sensitivity is illustrated in Figure 1, where decay curves of the phosphor $CdWO_4$ are shown at different temperatures. Decay-times spread over three orders of magnitude within the temperature sensitivity range of the phosphor, which is typically in the order of several hundred degrees.

$$I(t) = I_0 e^{-t/\tau} + C \quad (1)$$

The type of detector used may vary depending on the desired dimensionality of the temperature information. Photomultiplier tubes (PMT) are selected for zero-dimensional phosphor thermometry using the phosphorescence decay-time relation to temperature. The introduction of fast CMOS cameras opened the door for two-dimensional temperature measurements using the decay time method. In the past few years, several papers have reported the usage of fast CMOS cameras to obtain spatially and temporally resolved two-dimensional temperature maps inside internal combustion engines [13, 16, 17]. For a stack of camera images, the signal decrease in every pixel is later fitted to equation (1) in order to describe the decay of pixel intensities. Different fitting algorithms are available for obtaining the parameters of equation (1). Comparisons were made among the different algorithms to characterize their precision, accuracy and computational time, their results showing that the linear regression of the sum (LRS) algorithm exhibited similar accuracy and precision as that obtained by the nonlinear least-squares algorithm [21-23]. In this study, the trust-region reflective algorithm, a least-squares minimization algorithm, available in MATLAB was used due to its robustness.

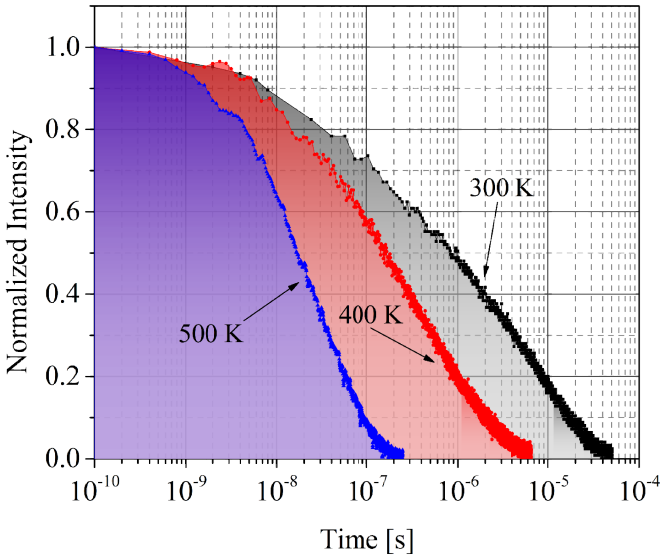

Figure 1. Phosphorescence decay curves of $CdWO_4$ phosphor at 300, 400 and 500 K.

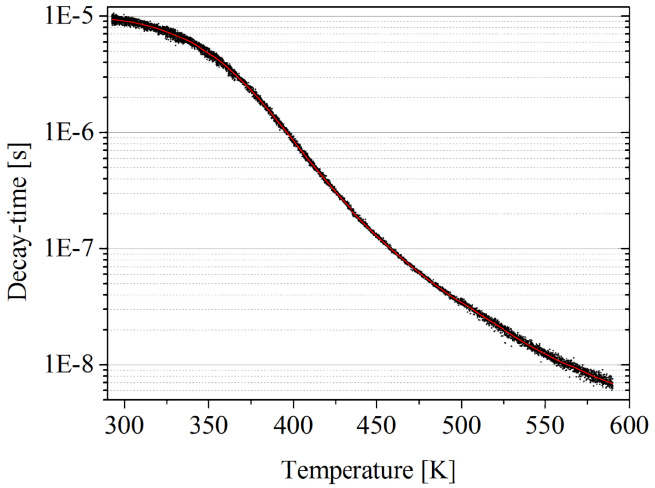

Figure 2. Temperature Calibration curve of $CdWO_4$. Calibration curve was constructed by automatic calibration routine [24].

To deduce the temperature from a decay-time, a calibration curve describing the relation between the phosphorescence decay-time and temperature must be built. A calibration curve for $CdWO_4$, shown in Figure 2, was acquired using an automatic calibration routine developed by the authors [24]. Decay-times of $CdWO_4$ exhibit a high sensitivity to temperatures within the 290-580 K range, which covers the range of expected temperatures of the cylinder wall of the engine. From earlier experiments conducted by the authors, $CdWO_4$ decay-time has shown to have a slight dependence on the laser fluence. A single-shot precision of around 2 K is obtained from the automatic calibration routine, while

considering an accuracy of 1.5 K reported by the manufacturer of the thermocouples.

Detector Linearity

Photodetectors are used to convert the transient phosphorescence decay into an electric signal to be measured by an oscilloscope. Special attention must be paid to ensure that the detector used is behaving linearly under the prevailing conditions. Severe signal distortions can occur to the measured signal if the detector is operating in its nonlinear region. The importance of detector linearity in phosphor thermometry was characterized and reported by Knappe et al. [25, 26]. The studies showed that photodetectors can severely distort the shape of the exponentially decaying signals. These distortions are mainly influenced by electronic gain, light intensity, and distinct properties of photodetectors. Depending on the electrical gain and the light intensity, the calculated decay times manifested variations up to a factor of three at a specific temperature. The magnitude of variations indicates that signal intensity compensation by detector gain modifications would heavily affect the calculated decay time and thus the measured temperature. In case detector gain change is necessary to compensate for low phosphorescence signal, different calibration curves must be acquired, each corresponding to the different detector settings implemented.

By testing an array of different photodetectors, the authors have identified a detector that provides superior linearity response among the tested photodetectors [26]. This detector is the Hamamatsu H11526-20-NF. Based on the conclusions of the linearity studies, the same detector was chosen for this measurement.

Phosphor coating thickness considerations

Applying thermographic phosphor in thermally unsteady environments requires extensive attention to phosphor coating thickness. Thermal gradients within the phosphor coating can lead to hidden inaccuracy of the measured temperature. A recent theoretical study reported by Atakan and Roskosch [27] showed that even very thin layers of phosphor coating could influence the maximum temperature measured during a transient combustion process, such as that occurring in combustion engines. Other factors like film absorptivity and conductivity also significantly affected the phosphor temperature. They have issued a recommendation to apply strongly absorbing films of thicknesses around 1μm.

Pilgrim et al [28] published another theoretical model predicting the temperature gradients as a function of thermal barrier coating (TBC) thickness. They reported that in the case of an unknown thermal gradient, a TBC of 20 μm thickness can manifest a maximum temperature variation of 7 K.

While previously presented studies dealt with the issue of thermal gradients within phosphor layer from a theoretical aspect, Knappe et al. [29, 30] presented experimental studies on this topic. The studies, presented by Knappe et al., were the first to characterize temperature variations induced by phosphor layer thickness. By applying coatings of different thicknesses onto a quartz liner of a homogeneous charge compression ignition engine and simultaneously exciting the front and back side of the phosphor layer, a comprehensive study of the effect of layer thickness could be performed. According to the study, spray coatings of thickness $\leq$ 20 μm did not show significant temperature gradients across the layer.

Although the thinnest possible layer is favored to avoid a temperature gradient within the coating, high phosphorescence emission intensity is required to obtain a good signal-to-noise ratio, especially in experimentally harsh environments like the ones present in a combustion engine. It all comes down to finding an optimum coating thickness that provides a compromise between temperature gradient minimization and adequate signal intensity.

Airbrush coating is a commonly used technique for the application of phosphor films onto the surface of interest. This technique provides thin and robust coatings that can endure typical in-cylinder conditions. The key aspect of airbrush coatings is the flexibility to apply coatings on a wide variation of surfaces with a great ease, giving it a significant advantage over other thin film deposition techniques like physical or chemical deposition. With care, sufficiently thin coatings can be sprayed satisfying the minimum thermal gradient requirement for reliable temperature measurements.

Automatic Phosphor Calibration

In previous work performed at Lund University, an automatic routine for calibration of thermographic phosphor was developed. The routine logs the phosphorescence decay signal and temperature simultaneously and continuously over the calibration temperature range. Compared to the conventional calibration method, the automated calibration introduced an improvement of 1-2 K to the overall accuracy of the calibration [24].

The generated phosphor calibration took the form of a database which was later used to develop a Signal Shape Recognition algorithm (SSR) for temperature extraction [31]. The SSR is a library-based algorithm that relies on the comparison of the measured exponential decay with the calibration database rather than fitting a theoretical model, usually a single exponential function, to the measured signal. By comparing the shape of the signals, uncertainty arising from an ill-imposed fit is avoided.

EXPERIMENTAL CONDITIONS

Engine Conditions

The engine used is a turbocharged low-speed two-stroke diesel engine, fully equipped for extensive testing. The main characteristic data of the 4T50ME-X engine in standard configuration is summarized in Table 1.

Table 1. 4T50ME-X research engine specifications.

Engine type	2-Stroke diesel
Number of cylinders	4

Bore [mm]	500
Stroke [m]	2.2
Stroke volume [l]	423
Compression ratio	14:1
Power [MW]	7
Max speed [rpm]	123
Max pressure [bar]	190

The engine is of the uniflow scavenged type, with air intake ports at the bottom of the cylinder and a centrally located exhaust valve at the top. The in-cylinder flow is defined by a strong swirling motion introduced with the scavenging air. In standard configuration, each cylinder is equipped with two separate fuel injectors, each having four nozzle holes. The fuel injection and exhaust valve systems are electronically controlled and hydraulically actuated. The cylinder used for optical testing can be independently controlled, and even motored by the remaining cylinders. The engine was operated on marine gas oil. For this study, one atomizer was employed on the test cylinder with a single 0.8 mm diameter nozzle hole.

Optical Access

Optical access to the top of the cylinder is obtained through a custom designed optical engine cover, see Figure 3 [32]. The optical engine cover features 24 ports, both from the top (10 vertical ports) and from the side (14 horizontal ports). Each of those ports can be used as either an optical port or fitted with a fuel injector. Unused ports are sealed with metal inserts. Inserts fitted with sapphire windows at the front are mounted into the ports and used for laser illumination and signal detection.

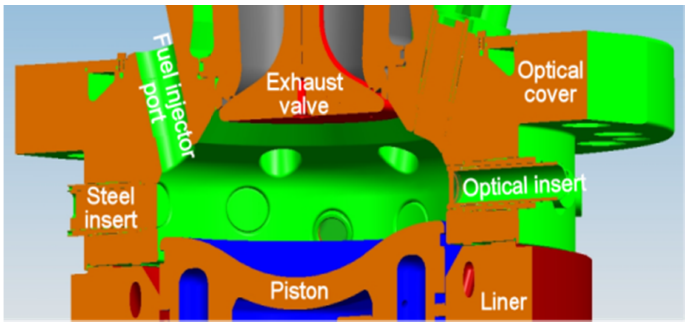

Figure 3. Schematic view of the optical cover installed on the engine (***green***: optical cover, ***dark red***: liner, ***blue***: piston, ***light red***: exhaust valve).

Experimental Setup

In this study, two optical ports were fitted with sapphire windows permitting for the excitation and collection of $CdWO_4$ phosphorescence. On the opposite side of the optical cylinder head, a cylinder wall insert was coated with $CdWO_4$ phosphor. The coating was shaped as a circular area with a diameter of 25 mm placed at the center of the 55 mm (in diameter) cylinder wall insert. The average thickness of the coating used in this work is measured to be around 20 µm, using a coating thickness gauge (Elcometer 456). The importance of the coating thickness factor was discussed earlier in the previous section.

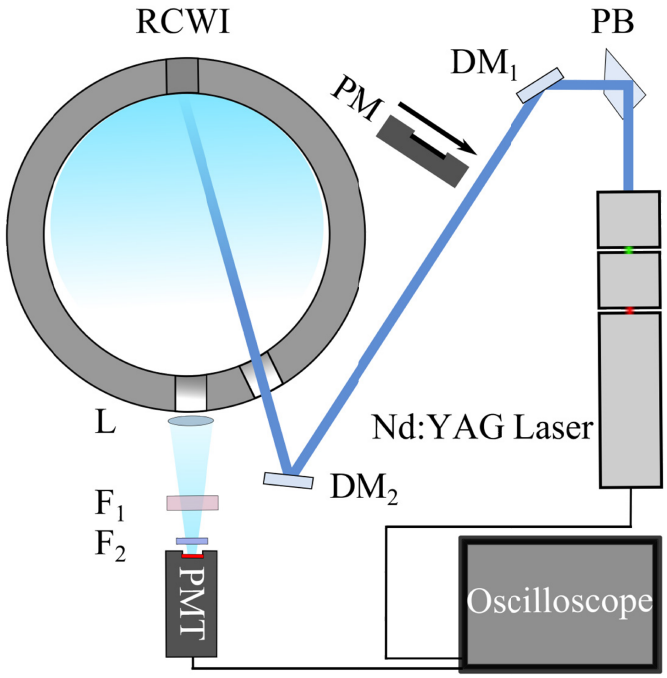

Figure 4. Experimental setup for phosphor thermography on the 4T50ME-X research engine platform. The Abbreviations represent the following, ***DM***: dichroic mirror, ***F1***: long-pass filter (λ>400 nm), ***F2***: Interference filter (center wavelength at 450 nm, 40 nm FWHM), ***L***: plano-convex lens (f = 100 mm), ***PB***: Pellin-Broca prism, ***PM***: laser power-meter, ***PMT***: photomultiplier tube, ***RCWI***: removable cylinder wall insert.

$CdWO_4$ was excited using the fourth harmonic, at 266 nm, of a pulsed Nd:YAG laser at a rate of 10 Hz. The temporal and spatial profile of the laser pulse is of Gaussian nature with a temporal full width at half maximum (FWHM) of 6 ns. Using a divergent lens, the laser beam is expanded from an initial diameter of 9 mm up to 60 mm at the phosphor coated cylinder wall to compensate for beam deviations induced by vigorous engine vibration and beam steering caused by thermal gradients. Due to the proximity of the setup to the engine, the thermally controlled fourth harmonic generation unit of the Nd:YAG laser would experience energy fluctuations. Thermally-induced laser energy drifts were minimized by placing the laser beneath a protective shell that utilized controlled air flow for thermal stabilization. The laser energy was stabilized around a value of 11 mJ per pulse throughout the entire measurement.

$CdWO_4$ has a broad phosphorescence emission centered around 470 nm [33]. An Interference filter centered at 450 nm with a FWHM of 40 nm was selected to spectrally narrow the detected phosphorescence. To further suppress any scattered laser radiation, a long-pass filter with a cutoff wavelength at 400 nm was mounted in front of the interference filter. A

Hamamatsu H11526-20-NF photomultiplier tube was used as the detector. An illustration of the complete setup is shown in Figure 4.

RESULTS AND DISCUSSION

To assess the validity of the phosphor thermometry technique in a large-bore engine, the wall temperature of one of the four cylinders was measured. The cylinder at which the measurements occurred was operated in two modes, fired mode and motored mode. In motored mode, the measurement cylinder was motored by use of the other three cylinders. In order to differentiate between different motoring conditions, the load at which the driving cylinders are operating at will be mentioned further on. The temperatures are plotted along with cylinder pressure versus crank-angle degrees (CAD). Top dead center (TDC) and bottom dead center (BDC) piston positions refer to 0 CAD and 180 CAD, respectively.

Large-bore engines run at relatively low speeds (typically up to 130 rpm). A single engine cycle would thus take about 0.5-1 second. By utilizing an advanced triggering system, the full potential of the 10 Hz laser can be exploited. This allows for several measurement events in a single cycle. The number of possible temperature measurements per cycle is governed by the engine speed. For engine speeds of 75 and 100 rpm, 8 and 6 measurement events were acquired per cycle achieving quasi-single cycle resolved temperature measurements. All of the temperatures presented are averaged over 50 single-shot measurements with error bars representing standard deviations.

Motored Engine Operation

The cycle-averaged wall temperatures obtained for motored operations are presented in Figure 5. Two engine loads were selected for the driving the cylinders (12% and 23% load). As mentioned earlier, the loads mentioned in this section refer to the loads at which the driving cylinders are operating. The temperature profile registered by the thermographic phosphor follows the trends observed by the pressure trace inside the cylinder. The increase in the standard deviation close to TDC can be attributed to lower signal due to beam steering caused by thermal gradients and increased flow turbulence. The variations seen in the temperature distribution is attributed to the fact that the engine temperature was not stable at the time of measurement. That led to a temperature difference between different sets of acquired measurements.

The registered baseline temperatures of the cylinder wall are constant around 435 K and 445 K for the 12% and 23% load. The peak temperatures registered were 449 K and 463. The volume of inlet air increases with increasing load, thus higher temperatures were observed at higher loads. A minor temperature drop is noticed around 120 CAD. This temperature drop is due to the expansion of the gases (exhaust blow down) and was estimated to be around 5 K.

To further analyze the results obtained at different loads, the baseline temperatures and the peak temperatures are compared. The baseline temperature obtained for the 23% load is about 10 K higher than that at 12% load. In addition, the peak temperature is almost 14 K higher than that at 12% load. The difference in the temperatures can be attributed to the increase in cylinder peak pressure and hence, gas temperature, at 23% load.

Temperature standard deviations averaged over 50 engine cycles are mostly within the order of 0.4-1.5 K, but larger temporal deviations of up to ±7 K are present at the measurement points close to the CADs corresponding to the opening of the exhaust valve. This could be due to the variations introduced by local turbulence created by this process [19].

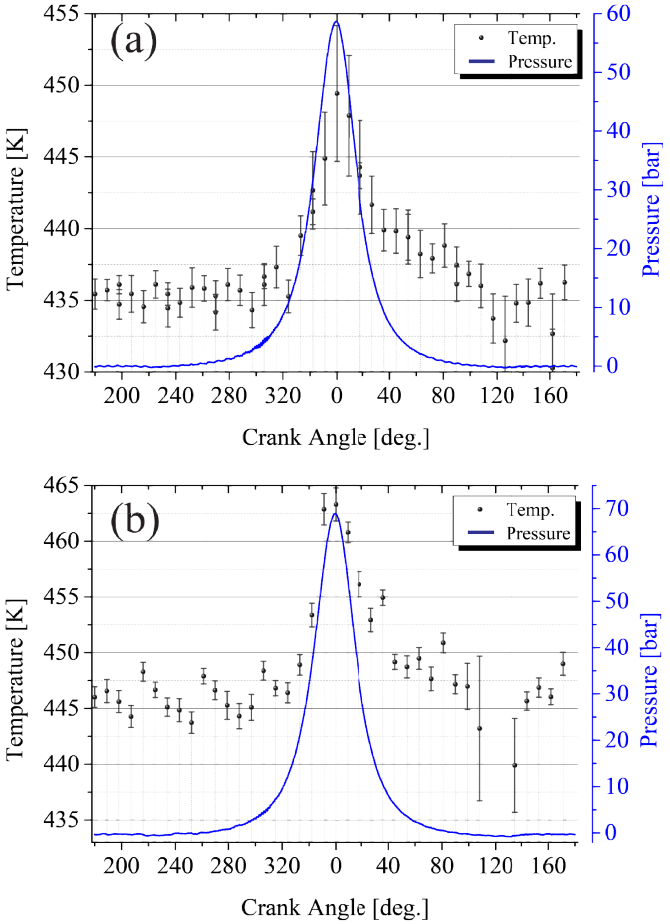

Figure 5. Average cylinder wall insert temperature as function of crank angle degrees for motored engine operation at driving cylinders load of ***(a)*** 12% (60 rpm) and ***(b)*** 23% (75 rpm) averaged over 50 engine cycles with the corresponding standard deviations.

Fired Engine Operation

Two main engine operating conditions were used for the fired engine operation and are listed in Table 2. The presented results in Figure 6 show the cylinder insert temperature measured at operating load of 23% (75 rpm) and 54% (100 rpm). The engine load and rpm were varied simultaneously to simulate a propeller load.

Table 2. Engine conditions during fired operation mode

Engine configuration	# 1	# 2
Load [%]	23	54
Engine speed [rpm]	75	100
Start of injection [CAD]	3	3
Injection duration [CAD]	10.3	13.7
Injection duration [ms]	22.9	22.9
Injected fuel [g/cycle]	1.61	1.65

Some of the measurements acquired just after the start of fuel injection (around 3 CAD) suffered from very low signal-to-noise ratio and were deemed unfit for temperature extraction. The drop in the signal-to-noise ratio is attributed to laser intensity and phosphorescence signal intensity attenuation by the sooty swirling flame inside the large-bore cylinder.

The peak temperatures reached were 470 K and 486 K for 23% and 54% load, respectively (presented in Fig. 6). The baseline temperatures were 450 K and 470 K, which is higher than the baseline temperatures obtained from the motored engine operation. The increase of the baseline temperatures is generated by the additional heat release from fuel combustion inside the cylinder. Standard deviations obtained for 50 cycles were around 2-3 K with the exception of the large standard deviations of ±8 K, seen during the opening of the exhaust valve. The peak cylinder pressures attained were 63 bar for 23% and 107 bar for 54% load. Thermographic phosphors show a high capability to provide accurate temperature measurements at high pressures.

CONCLUSIONS AND OUTLOOK

A feasibility study of using phosphor thermometry in a large-bore two-stroke marine engine is presented. The importance of aspects such as detector linearity and phosphor coating thickness for the accuracy of phosphor thermometry were discussed. The temperature of a phosphor-coated cylinder wall segment was effectively measured at different operating conditions. Wall temperatures were acquired under both motored and fired engine operations. Two different loads were selected for each operation mode covering the low to medium engine load range. Temporal standard deviations were within the 1-3 K range except near TDC where combustion is initiated, and around 120 CAD where significant changes in in-cylinder flow occurred due to exhaust blow-down process.

The present work has demonstrated the feasibility of in-situ surface temperature measurements in a running two-stroke marine diesel engine. One can envisage extending the approach demonstrated here to also measure the surface temperature of critical in-cylinder components, which can be hard to instrument with fast thermocouples. The exhaust valve, the piston and fuel injectors are examples of such components. This opens up the possibility for monitoring the cycle resolved surface temperature on critical in-cylinder components, such as the exhaust valve, as a function of engine operating parameters as well as fuel injector arrangement. Such novel information could assist in identifying areas where coatings of base materials of higher temperature capabilities should be applied. It could also assist in directing the layout of fuel injector nozzle hole directions in order to limit peak heat-loads on individual components.

Further temperature measurements using thermographic phosphors are planned in collaboration with MAN Diesel & Turbo on the 4T50ME-X running on natural gas. A single-optical fiber setup will be utilized to back-illuminate the phosphor coating and thus minimizing the effects of flame luminosity and soot deposition on the surface of the coating. The downsizing of optical access ports achieved by use of an optical fiber will also allow for temperature measurements at higher engine loads.

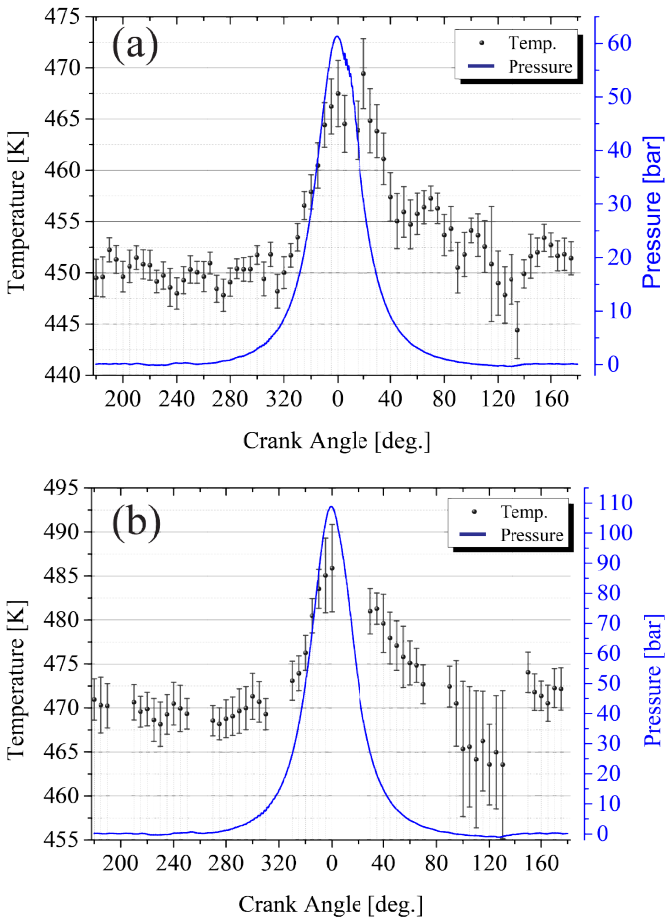

Figure 6. Average cylinder wall insert temperature as function of crank angle degrees for fired engine operation at ***(a)*** 23% load (75 rpm) and ***(b)*** 54% load (100 rpm) averaged over 50 engine cycles with the corresponding standard deviations.

ACKNOWLEDGEMENTS

The research leading to these results has received funding from the European Union Seventh Framework Programme (FP7/2007-2011) under grant agreement no. 265861 (Helios).

REFERENCES

[1] *International Shipping Facts and Figures – Information Resources on Trade, Safety, Security, Environment* M.K. Center, Editor 2012, International Maritime Organization.

[2] L. Juliusen, S. Mayer, and M. Kryger, *The MAN ME-GI engine: From initial system considerations to implementation and performance optimisation*, in *CIMAC Congress* 2013: Shanghai, China.

[3] K.G. Kreider, *Thin film thermocouples for internal combustion engines.* Journal of Vacuum Science & Technology A, 1986. **4**(6): p. 2618-2623.

[4] Y. Heichal, S. Chandra, and E. Bordatchev, *A fast-response thin film thermocouple to measure rapid surface temperature changes.* Experimental Thermal and Fluid Science, 2005. **30**(2): p. 153-159.

[5] M.A. Marr, J.S. Wallace, S. Chandra, L. Pershin, and J. Mostaghimi, *A fast response thermocouple for internal combustion engine surface temperature measurements.* Experimental Thermal and Fluid Science, 2010. **34**(2): p. 183-189.

[6] C.A. Christiansen, S. Mayer, and J. Schramm, *Simultaneous Transient Surface Temperature and Heat Flux Measurements in a Large Bore Two-Stroke Diesel Engine*, in *Proceedings of the ASME 2012 Internal Combustion Engine Division Fall Technical Conference (ICEF 2012)*2012, American Society of Mechanical Engineers.

[7] S.W. Allison and G.T. Gillies, *Remote thermometry with thermographic phosphors: Instrumentation and applications.* Review of Scientific Instruments, 1997. **68**(7): p. 2615-2650.

[8] A. Khalid and K. Kontis, *Thermographic Phosphors for High Temperature Measurements: Principles, Current State of the Art and Recent Applications.* Sensors, 2008. **8**(9): p. 5673-5744.

[9] M. Aldén, A. Omrane, M. Richter, and G. Särner, *Thermographic phosphors for thermometry: A survey of combustion applications.* Progress in Energy and Combustion Science, 2011. **37**(4): p. 422-461.

[10] J. Brübach, C. Pflitsch, A. Dreizler, and B. Atakan, *On surface temperature measurements with thermographic phosphors: A review.* Progress in Energy and Combustion Science, 2013. **39**(1): p. 37-60.

[11] G. Särner, M. Richter, M. Aldén, A. Vressner, and B. Johansson, *Cycle Resolved Wall Temperature Measurements Using Laser-Induced Phosphorescence in an HCCI Engine.* SAE Technical Paper, 2005. **2005-01-3870**.

[12] C. Wilhelmsson, A. Vressner, P. Tunestål, B. Johansson, G. Särner, and M. Aldén, *Combustion Chamber Wall Temperature Measurement and Modeling During Transient HCCI Operation.* SAE Technical Paper, 2005. **2005-01-3731**.

[13] S. Someya, M. Uchida, K. Tominaga, H. Terunuma, Y. Li, and K. Okamoto, *Lifetime-based phosphor thermometry of an optical engine using a high-speed CMOS camera.* International Journal of Heat and Mass Transfer, 2011. **54**(17–18): p. 3927-3932.

[14] N. Fuhrmann, E. Baum, J. Brubach, and A. Dreizler, *High-speed phosphor thermometry.* Review of Scientific Instruments, 2011. **82**(10): p. 104903-4.

[15] N. Fuhrmann, C. Litterscheid, C.P. Ding, J. Brübach, B. Albert, and A. Dreizler, *Cylinder head temperature determination using high-speed phosphor thermometry in a fired internal combustion engine.* Applied Physics B, 2013: p. 1-11.

[16] S. Someya, Y. Okura, T. Munakata, and K. Okamoto, *Instantaneous 2D imaging of temperature in an engine cylinder with flame combustion.* International Journal of Heat and Mass Transfer, 2013. **62**(0): p. 382-390.

[17] N. Fuhrmann, M. Schneider, C.P. Ding, J. Brübach, and A. Dreizler, *Two-dimensional surface temperature diagnostics in a full-metal engine using thermographic phosphors.* Measurement Science and Technology, 2013. **24**(9): p. 095203.

[18] N.J. Neal, J. Jordan, and D. Rothamer, *Simultaneous Measurements of In-Cylinder Temperature and Velocity Distribution in a Small-Bore Diesel Engine Using Thermographic Phosphors.* SAE Int. J. Engines, 2013. **6**(1): p. 300-318.

[19] J. Hult, S. Matlok, and S. Mayer, *Particle image velocimetry measurements of swirl and scavenging in a large marine two-stroke Diesel engine.* SAE Int. J. Engines, 2014(2014-01-1173).

[20] J. Hult, S. Matlok, and S. Mayer, *Optical Diagnostics of Fuel Injection and Ignition in a Marine Two-Stroke Diesel Engine.* SAE Int. J. Engines, 2014(7:2014-01-1448).

[21] C. Moore, S.P. Chan, J.N. Demas, and B.A. DeGraff, *Comparison of Methods for Rapid Evaluation of Lifetimes of Exponential Decays.* Applied Spectroscopy, 2004. **58**(5): p. 603-607.

[22] M.A. Everest and D.B. Atkinson, *Discrete sums for the rapid determination of exponential decay constants.* Review of Scientific Instruments, 2008. **79**(2): p. 023108 - 023108-9.

[23] N. Fuhrmann, J. Brübach, and A. Dreizler, *On the mono-exponential fitting of phosphorescence decays.* Applied Physics B, 2013: p. 1-11.

[24] F. Abou Nada, C. Knappe, X. Xu, M. Richter, and M. Aldén, *Development of an automatic routine for calibration of thermographic phosphors.* Measurement Science and Technology, 2014. **25**(2): p. 025201.

[25] C. Knappe, J. Linden, F. Abou Nada, M. Richter, and M. Alden, *Investigation and compensation of the nonlinear response in photomultiplier tubes for quantitative single-shot measurements.* Review of Scientific Instruments, 2012. **83**(3): p. 034901-7.

[26] C. Knappe, F. Abou Nada, M. Richter, and M. Alden, *Comparison of photo detectors and operating conditions for decay time determination in phosphor thermometry*. Review of Scientific Instruments, 2012. **83**(9): p. 094901-10.

[27] B. Atakan and D. Roskosch, *Thermographic phosphor thermometry in transient combustion: A theoretical study of heat transfer and accuracy*. Proceedings of the Combustion Institute, 2013. **34**(2): p. 3603-3610.

[28] C.C. Pilgrim, J.P. Feist, and A.L. Heyes, *On the effect of temperature gradients and coating translucence on the accuracy of phosphor thermometry*. Measurement Science and Technology, 2013. **24**(10): p. 105201.

[29] C. Knappe, P. Andersson, M. Algotsson, M. Richter, J. Linden, M. Alden, M. Tuner, and B. Johansson, *Laser-Induced Phosphorescence and the Impact of Phosphor Coating Thickness on Crank-Angle Resolved Cylinder Wall Temperatures*. SAE Int. J. Engines, 2011. **4**(1): p. 1689-1698.

[30] C. Knappe, M. Algotsson, P. Andersson, M. Richter, M. Tunér, B. Johansson, and M. Aldén, *Thickness dependent variations in surface phosphor thermometry during transient combustion in an HCCI engine*. Combustion and Flame, 2013. **160**(8): p. 1466-1475.

[31] C. Knappe, K. Pfeiffer, M. Richter, and M. Aldén, *A library-based algorithm for evaluation of luminescent decay curves by shape recognition in time domain phosphor thermometry*. Journal of Thermal Analysis and Calorimetry, 2013. **115**(1): p. 545-554.

[32] J. Hult and S. Mayer, *A methodology for laser diagnostics in large-bore marine two-stroke diesel engines*. Measurement Science and Technology, 2013. **24**(4): p. 045204.

[33] G. Särner, M. Richter, and M. Aldén, *Investigations of blue emitting phosphors for thermometry*. Measurement Science and Technology, 2008. **19**(12): p. 125304.